On the determination of hole subband structure for quantum well systems with arbitrary growth direction

1999 J. Phys.: Condens. Matter 11 4021

(http://iopscience.iop.org/0953-8984/11/20/308)

J. Phys.: Condens. Matter **11** (1999) 4021–4030. Printed in the UK PII: S0953-8984(99)00474-9

On the determination of hole subband structure for quantum well systems with arbitrary growth direction

M Kucharczyk†, J Taylor† and M S Wartak‡§

† Department of Physics and Computing, Wilfrid Laurier University, Waterloo, Ontario, Canada N2L 3C5

‡ Semilab, Department of Physics, Tampere University of Technology, PO Box 692, Tampere, FIN-33101, Finland

Received 31 December 1998

Abstract. We have generalized the plane-wave method used by Mathine *et al* (Mathine D L, Myjak S K and Maracas G N 1995 *IEEE J. Quantum Electron.* **31** 1216–22) for electrons to the case of light and heavy holes in quantum well systems with an arbitrary growth direction. Our method allows for relaxing the assumption of constant Luttinger parameters as used by Xia (Xia J-B 1991 *Phys. Rev.* B **43** 9856–64) and remains valid when the parameters experience discontinuities across the heterointerface. Although the method has been thoroughly tested for rectangular quantum wells only, it can be equally well applied to quantum wells of other shapes also.

1. Introduction

During the process of simulation of QW semiconductor lasers, one needs fast and reliable methods of solving the eigenvalue problem for the effective-mass Luttinger–Kohn (LK) Hamiltonian. The most straightforward methods can be reduced, in principle, to searching for zeros of—as a rule—an extremely strongly varying function resulting from matching the boundary conditions at the barrier–well interfaces. The function is in fact a determinant of a 4×4, 8×8, or 16×16 complex matrix, the elements of which contain different combinations of exponential functions of the wave-vector components and energy. Obtaining the determinant function is substantially simplified by using analytical expressions for the envelope functions given by Andreani *et al* [1], but the problem of finding zeros of the function in the case of an arbitrary direction of growth remains very difficult and numerically unstable.

In the case of the growth direction $\langle 001\rangle$, where the effective-mass Hamiltonian can be block diagonalized [2, 3], one is fortunate enough to encounter only a 4×4 determinant. For the majority of other directions of growth, an attempt at block diagonalization would lead to messy and impossible-to-handle blocks containing, at best, combinations of the operators $\partial/\partial\zeta$ and $\partial^2/\partial\zeta^2$ under the square root. Generally speaking, the straightforward methods encounter difficulties due to strong variation of the search function, which originates from the exponential character of the solutions.

The finite-difference method used in reference [4] does not need any sophisticated search function, and at its final stage includes a simple diagonalization of a larger or smaller matrix.

§ Permanent address: Department of Physics and Computing, Wilfrid Laurier University, Waterloo, Ontario, Canada N2L 3C5.

It was successfully used by Meney [5, 6] in valence subband-structure calculations for GaAs–$Al_xGa_{1-x}As$ quantum wells for four different growth directions. However, the method raises the question of computational stability, as a result of the replacement of derivatives with finite differences, as well as that of the behaviour of the envelope functions in the barrier far from the interface (where should they vanish?) These are unnecessary complications, given the linearity of the differential equations in the eigenvalue problem under consideration.

Los *et al* [7] gave a general theoretical description of the 8×8 (conduction band, heavy-hole band, light-hole band, split-off band) $\vec{k} \cdot \vec{p}$ approach for determining the band structure of quantum well semiconductor systems for any growth direction. To solve the effective-mass equation they used the finite-element method, which has the advantage over the finite-difference method that it takes into account 'exactly' the interface discontinuities of the potential and of the band parameters, and 'correctly' matches the envelope functions at the interfaces

As indicated by Altarelli *et al* [8] in their study of GaAs–AlGaAs quantum wells by the variational method [9], in the subband-structure calculations one can consider a superlattice instead of an actual single quantum well, since when the barrier thickness is large enough the isolated-well results are recovered. The plane-wave (PW) expansion method of Xia [10] when applied to a superlattice with very thick barriers should then give the subband structure of a corresponding isolated quantum well. Although Xia applied the PW method to a range of growth directions, his calculations suffered from serious limiting assumptions about the constancy of the Luttinger parameters ($\gamma_j,\ j = 1, 2, 3$) across the well–barrier interface. Consequently the calculations are valid only when the changes of the parameters γ_j across the interface are very small.

Recently, we have undertaken a systematic study of the effects of the growth orientation on the performance of QW semiconductor lasers. In [11] we have reported the results of effective-mass calculations using the PW method with $\gamma_j = \text{constant}_j$. Here we describe an easy method for carrying out quantum well subband-structure calculations based on the effective-mass LK Hamiltonian. The method is the result of a generalization of the plane-wave method used by Mathine *et al* [12] for electrons in the conduction band to the case of holes in the valence band, with a simultaneous relinquishing of the assumption of constant γ_j used in reference [10].

The objective of the present paper is the description of the method, which has the following two advantages:

(a) it is fast and numerically stable for all directions of growth; and

(b) it works well when the Luttinger parameters experience discontinuities across the well–barrier interface.

2. Description of the method

Let us consider a Cartesian system of coordinates with the x-axis pointing in the crystallographic direction (100), the y-axis in the direction (010), and the z-axis in the direction (001). If we rotate the system of coordinates to a new position, the z-axis becomes a new axis, the ζ-axis, the y-axis becomes a new axis, the η-axis, and x at the new position can be referred to as ξ. The new orientation of the coordinate system (ξ, η, ζ) can be determined by the angle θ between ζ- and z-axes and the angle φ between the projection of the ζ-axis onto the x–y plane and the old x-axis.

The heterointerfaces of a quantum well structure grown in the direction of the ζ-axis are then parallel to the ξ–η plane. The motion of holes in such a structure can be described by the following 4×4 effective-mass Hamiltonian (in units where $\hbar^2/(2m_0) = 1$):

$$\hat{H} = \gamma_1(\zeta)\mathbf{I}(k_1^2 + k_2^2 + \hat{k}_3^2) + \mathbf{I}V(\zeta) + \gamma_2(\zeta)(\mathbf{A}k_1^2 + \mathbf{B}k_2^2 + \mathbf{C}\hat{k}_3^2 + \mathbf{D}k_1k_2 + \mathbf{E}k_1\hat{k}_3 + \mathbf{F}k_2\hat{k}_3) \\ + \gamma_3(\zeta)(\mathbf{A}^1k_1^2 + \mathbf{B}^1k_2^2 + \mathbf{C}^1\hat{k}_3^2 + \mathbf{D}^1k_1k_2 + \mathbf{E}^1k_1\hat{k}_3 + \mathbf{F}^1k_2\hat{k}_3) \quad (1)$$

where for a square quantum well

$$V(\zeta) = \begin{cases} 0 & \text{if } |\zeta| < L_w/2 \\ \Delta E_v & \text{if } |\zeta| \geqslant L_w/2 \end{cases} \quad (2a)$$

and

$$\gamma_j(\zeta) = \begin{cases} \gamma_j^w & \text{if } |\zeta| < L_w/2 \\ \gamma_j^b & \text{if } |\zeta| \geqslant L_w/2 \end{cases} \qquad j \in \{1, 2, 3\}. \quad (2b)$$

Here L_w is the quantum well width, ΔE_v is the valence band discontinuity, and γ_j^w and γ_j^b are the Luttinger parameters of the well and of the barrier materials. $\mathbf{A}, \ldots, \mathbf{F}, \mathbf{A}^1, \ldots, \mathbf{F}^1$ are 4×4 matrices with matrix elements dependent on θ and φ, $\mathbf{I}$ is the 4×4 identity matrix, and $\hat{k}_3 = -\mathrm{i}\,\partial/\partial\zeta$.

The Hamiltonian (1) was derived by Xia [10] with $\mathbf{A}, \ldots, \mathbf{F}, \mathbf{A}^1, \ldots, \mathbf{F}^1$ given as functions of the angle θ only (only $\varphi = 45^\circ$ was considered). The effective-mass equation resulting from equation (1) was solved in [10] with the limiting assumption that the Luttinger parameters did not change across the well–barrier interface ($\gamma_j(\zeta) = \text{constant}_j$). In the appendix and table 1 we give the matrices $\mathbf{A}, \ldots, \mathbf{F}, \mathbf{A}^1, \ldots, \mathbf{F}^1$ for an arbitrary direction of growth specified by both angles θ and φ.

In the present work, the effective-mass equation

$$\hat{H}\mathcal{F}(\zeta) = E\mathcal{F}(\zeta) \quad (3)$$

where $\mathcal{F}(\zeta) = [\mathcal{F}_{3/2}(\zeta), \mathcal{F}(\zeta)_{1/2}, \mathcal{F}(\zeta)_{-1/2}, \mathcal{F}(\zeta)_{-3/2}]$ is the ζ-part of the envelope function, was solved for $\gamma_j(\zeta)$ given in (2b), i.e. without the limiting assumption requiring constant Luttinger parameters that was employed in [10].

We replaced a single quantum well by a periodic pattern of wells separated by very thick barriers: $L_b = 10L_w$. The envelope functions $\mathcal{F}_\alpha(\zeta)$, where $\alpha \in \{3/2, 1/2, -1/2, -3/2\}$, the Luttinger parameters $\gamma_j(\zeta)$, as well as the potential $V(\zeta)$ were expanded into series of N plane waves:

$$\mathcal{F}_\alpha(\zeta) = \sum_{n=-(N-1)/2}^{(N-1)/2} f_{\alpha,n} \frac{1}{\sqrt{L}} \mathrm{e}^{\mathrm{i}(2\pi n/L)\zeta} \quad (4a)$$

$$\gamma_j(\zeta) = \sum_{m=-(N-1)}^{N-1} \gamma_{j,m} \frac{1}{\sqrt{L}} \mathrm{e}^{\mathrm{i}(2\pi m/L)\zeta} \qquad j \in \{1, 2, 3\} \quad (4b)$$

and

$$V(\zeta) = \sum_{m=-(N-1)}^{N-1} V_m \frac{1}{\sqrt{L}} \mathrm{e}^{\mathrm{i}(2\pi m/L)\zeta} \quad (4c)$$

where $f_{\alpha,n}$ are unknown coefficients independent of ζ,

$$\gamma_{j,m} = \frac{1}{\sqrt{L}} \int_{-L/2}^{L/2} \mathrm{e}^{-\mathrm{i}(2\pi m/L)\zeta} \gamma_j(\zeta)\,\mathrm{d}\zeta \quad (5a)$$

and

$$V_m = \frac{1}{\sqrt{L}} \int_{-L/2}^{L/2} \mathrm{e}^{-\mathrm{i}(2\pi m/L)\zeta} V(\zeta)\,\mathrm{d}\zeta. \quad (5b)$$

Table 1. Matrix elements of the 12 matrices in the Luttinger–Kohn Hamiltonian (1). See the appendix.

$A_{1,1} = -6c_\theta^2 s_\theta^2 \left[c_\varphi^4 + s_\varphi^2\right] + 1$
$A_{1,2} = -2\sqrt{3} c_\theta s_\theta \left[2c_\theta^2(c_\varphi^4 + s_\varphi^2) - 1 + \mathrm{i} c_\theta c_\varphi s_\varphi (2c_\varphi^2 - 1)\right]$
$A_{1,3} = -2\sqrt{3} c_\theta^2 \left[c_\theta^2(c_\varphi^4 + s_\varphi^2) + (c_\varphi^4 - c_\varphi^2 - 1) + \mathrm{i} c_\theta c_\varphi s_\varphi (2c_\varphi^2 - 1)\right] - \sqrt{3}$
$B_{1,1} = -6c_\varphi^2 s_\theta^2 s_\varphi^2 + 1$
$B_{1,2} = -2\sqrt{3} c_\varphi s_\theta \left[2c_\theta c_\varphi s_\varphi^2 - \mathrm{i} s_\varphi (2c_\varphi^2 - 1)\right]$
$B_{1,3} = -2\sqrt{3} c_\varphi \left[c_\varphi s_\varphi^2 (c_\theta^2 + 1) - \mathrm{i} c_\theta s_\varphi (2c_\varphi^2 - 1)\right] + \sqrt{3}$
$C_{1,1} = 6s_\theta^2 \left[c_\theta^2(1 - c_\varphi^2 s_\varphi^2) + c_\varphi^2 s_\varphi^2\right] - 2$
$C_{1,2} = 2\sqrt{3} s_\theta \left[2c_\theta c_\varphi^2 s_\theta^2 s_\varphi^2 + c_\theta (2c_\theta^2 - 1) - \mathrm{i} c_\varphi s_\varphi s_\theta^2 (2c_\varphi^2 - 1)\right]$
$C_{1,3} = -2\sqrt{3} s_\theta^2 \left[c_\theta^2(c_\varphi^4 + s_\varphi^2) - c_\varphi^2 s_\varphi^2 + \mathrm{i} c_\theta c_\varphi s_\varphi (2c_\varphi^2 - 1)\right]$
$D_{1,1} = 6c_\theta s_\theta^2 c_\varphi s_\varphi (2c_\varphi^2 - 1)$
$D_{1,2} = 4\sqrt{3} c_\theta s_\theta c_\varphi \left[c_\theta s_\varphi (2c_\varphi^2 - 1) + \mathrm{i}\, 2c_\varphi s_\varphi^2\right]$
$D_{1,3} = 2\sqrt{3} c_\theta c_\varphi \left[s_\varphi (c_\theta^2 + 1)(2c_\varphi^2 - 1) + \mathrm{i}\, 4c_\theta c_\varphi s_\varphi^2\right]$
$E_{1,1} = 6s_\theta c_\theta \left[2c_\varphi^2 s_\theta^2 s_\varphi^2 + 2c_\theta^2 - 1\right]$
$E_{1,2} = -4\sqrt{3} c_\theta s_\theta^2 \left[2c_\theta (c_\varphi^4 + s_\varphi^2) + \mathrm{i} c_\varphi s_\varphi (2c_\varphi^2 - 1)\right]$
$E_{1,3} = 2\sqrt{3} c_\theta s_\theta \left[2c_\varphi^2 s_\varphi^2 (1 + c_\theta^2) + 1 - 2c_\theta^2 + \mathrm{i}\, 2c_\theta c_\varphi s_\theta (1 - 2c_\varphi^2)\right]$
$F_{1,1} = 6c_\varphi s_\theta^3 s_\varphi (2c_\varphi^2 - 1)$
$F_{1,2} = 4\sqrt{3} c_\varphi s_\theta^2 \left[c_\theta s_\varphi (2c_\varphi^2 - 1) + \mathrm{i}\, 2c_\varphi s_\varphi^2\right]$
$F_{1,3} = 2\sqrt{3} s_\theta c_\varphi \left[s_\varphi (2c_\varphi^2 - 1)(1 + c_\theta^2) + \mathrm{i}\, 4c_\theta c_\varphi s_\varphi^2\right]$
$A_{1,1}^1 = 6c_\theta^2 s_\varphi^2 (c_\varphi^4 + s_\varphi^2)$
$A_{1,2}^1 = 2\sqrt{3} c_\theta s_\theta \left[2c_\theta^2(c_\varphi^4 + s_\varphi^2) - 1 + \mathrm{i} c_\theta c_\varphi s_\varphi (2c_\varphi^2 - 1)\right]$
$A_{1,3}^1 = 2\sqrt{3} c_\theta^2 \left[c_\theta^2(c_\varphi^4 + s_\varphi^2) + (c_\varphi^4 - c_\varphi^2 - 1) + \mathrm{i} c_\theta c_\varphi s_\varphi (2c_\varphi^2 - 1)\right]$
$B_{1,1}^1 = 6c_\varphi^2 s_\theta^2 s_\varphi^2$
$B_{1,2}^1 = 2\sqrt{3} s_\theta c_\varphi \left[2c_\theta c_\varphi s_\varphi^2 - \mathrm{i} s_\varphi (1 - 2c_\varphi^2)\right]$
$B_{1,3}^1 = 2\sqrt{3} c_\varphi \left[c_\varphi s_\varphi^2 (c_\theta^2 + 1) + \mathrm{i} c_\theta s_\varphi (1 - 2c_\varphi^2)\right]$
$C_{1,1}^1 = -6s_\theta^2 \left[c_\theta^2(1 - c_\varphi^2 s_\varphi^2) + c_\varphi^2 s_\varphi^2\right]$
$C_{1,2}^1 = -2\sqrt{3} s_\theta \left[2c_\theta c_\varphi^2 s_\theta^2 s_\varphi^2 + c_\theta (2c_\theta^2 - 1) - \mathrm{i} c_\varphi s_\varphi s_\theta^2 (2c_\varphi^2 - 1)\right]$
$C_{1,3}^1 = 2\sqrt{3} s_\theta^2 \left[c_\theta^2(c_\varphi^4 + s_\varphi^2) - c_\varphi^2 s_\varphi^2 + \mathrm{i} c_\theta c_\varphi s_\varphi (2c_\varphi^2 - 1)\right]$
$D_{1,1}^1 = 6c_\theta s_\theta^2 c_\varphi s_\varphi (1 - 2c_\varphi^2)$
$D_{1,2}^1 = 4\sqrt{3} c_\theta s_\theta c_\varphi \left[c_\theta s_\varphi (1 - 2c_\varphi^2) - \mathrm{i}\, 2c_\varphi s_\varphi^2\right]$
$D_{1,3}^1 = 2\sqrt{3} c_\theta c_\varphi \left[s_\varphi (c_\theta^2 + 1)(1 - 2c_\varphi^2) - \mathrm{i}\, 4c_\theta c_\varphi s_\varphi^2\right] + \mathrm{i}\, 2\sqrt{3}$
$E_{1,1}^1 = -6s_\theta c_\theta \left[2c_\varphi^2 s_\theta^2 s_\varphi^2 + 2c_\theta^2 - 1\right]$
$E_{1,2}^1 = 4\sqrt{3} c_\theta s_\theta^2 \left[2c_\theta (c_\varphi^4 + s_\varphi^2) + \mathrm{i} c_\varphi s_\varphi (2c_\varphi^2 - 1)\right] - 2\sqrt{3}$
$E_{1,3}^1 = -2\sqrt{3} c_\theta s_\theta \left[2c_\varphi^2 s_\varphi^2 (1 + c_\theta^2) + 1 - 2c_\theta^2 + \mathrm{i}\, 2c_\theta c_\varphi s_\theta (1 - 2c_\varphi^2)\right]$
$F_{1,1}^1 = 6c_\varphi s_\theta^3 s_\varphi (1 - 2c_\varphi^2)$
$F_{1,2}^1 = -4\sqrt{3} c_\varphi s_\theta^2 \left[c_\theta s_\varphi (2c_\varphi^2 - 1) + \mathrm{i}\, 2c_\varphi s_\varphi^2\right] + 2\mathrm{i}\sqrt{3}$
$F_{1,3}^1 = -2\sqrt{3} s_\theta c_\varphi \left[s_\varphi (2c_\varphi^2 - 1)(1 + c_\theta^2) + \mathrm{i}\, 4c_\theta c_\varphi s_\varphi^2\right]$

The plane-wave expansions (4*a*)–(4*c*) were substituted into equation (3). Next the system of four equations (3) was multiplied on both sides from the left by $(1/\sqrt{L})\mathrm{e}^{-\mathrm{i}(2\pi n'/L)\zeta}$, where $-(N-1)/2 \leqslant n' \leqslant (N-1)/2$, and each term was integrated over ζ from $-L/2$ to $L/2$. This gave a system of $4N$ linear equations for the coefficients $f_{\alpha,n}$ in the expansion of the envelope functions (4*a*), as the effective-mass Hamiltonian was represented by the matrix

$$\begin{aligned} H_{\alpha\beta,n'n} = L^{-1/2}\Bigg\{ & \gamma_{1,n'-n}\delta_{\alpha\beta}\left(k_1^2 + k_2^2 + \frac{4\pi^2 n'n}{L^2}\right) + \delta_{\alpha\beta}V_{n'-n} \\ & + \gamma_{2,n'-n}\Bigg[A_{\alpha\beta}k_1^2 + B_{\alpha\beta}k_2^2 + C_{\alpha\beta}\frac{4\pi^2 n'n}{L^2} + D_{\alpha\beta}k_1k_2 + E_{\alpha\beta}k_1\frac{\pi(n'+n)}{L} \\ & + F_{\alpha\beta}k_2\frac{\pi(n'+n)}{L}\Bigg] + \gamma_{3,n'-n}\Bigg[A^1_{\alpha\beta}k_1^2 + B^1_{\alpha\beta}k_2^2 + C^1_{\alpha\beta}\frac{4\pi^2 n'n}{L^2} + D^1_{\alpha\beta}k_1k_2 \\ & + E^1_{\alpha\beta}k_1\frac{\pi(n'+n)}{L} + F^1_{\alpha\beta}k_2\frac{\pi(n'+n)}{L}\Bigg]\Bigg\} \end{aligned} \tag{6}$$

where $\alpha, \beta \in \{3/2, 1/2, -1/2, -3/2\}$ and $\delta_{\alpha\beta}$ is the Kronecker delta.

The appearance in equation (6) of $\gamma_{j,n'-n}$ and of $V_{n'-n}$ explains the different summation limits in equations (4*b*) and (4*c*) as compared to equation (4*a*). Whereas n and n' take N different values (between $-(N-1)/2$ and $(N-1)/2$), $n'-n$ takes $2N$ different values (between $-(N-1)$ and $N-1$).

To ensure the hermiticity of this Hamiltonian matrix, we replaced the operator $\gamma_j(\zeta)\hat{k}_3^2$ which appears in equation (1) as follows:

$$\gamma_j(\zeta)\hat{k}_3^2 = -\gamma_j(\zeta)\frac{\partial^2}{\partial\zeta^2} \qquad \text{with } -\frac{\partial}{\partial\zeta}\gamma_j(\zeta)\frac{\partial}{\partial\zeta} \tag{7}$$

and also

$$\gamma_j(\zeta)\hat{k}_3 = -\mathrm{i}\gamma_j(\zeta)\frac{\partial}{\partial\zeta} \qquad \text{with } -\frac{\mathrm{i}}{2}\left[\gamma_j(\zeta)\frac{\partial}{\partial\zeta} + \frac{\partial}{\partial\zeta}\gamma_j(\zeta)\right]. \tag{8}$$

Compare for example [2].

The chosen replacement of $\gamma_j(\zeta)\hat{k}_3$ and $\gamma_j(\zeta)\hat{k}_3^2$ corresponds to the approach of Altarelli *et al* [8, 9] in which the envelope function and the probability current density are continuous across each interface ('conventional' boundary conditions). It must be emphasized that this is not the only way of ensuring hermiticity of the Hamiltonian. The replacement of $\gamma_j(\zeta)\hat{k}_3^2$ by

$$-\gamma_j^a(\zeta)\frac{\partial}{\partial\zeta}\gamma_j^b(\zeta)\frac{\partial}{\partial\zeta}\gamma_j^a(\zeta) \qquad \text{with } 2a + b = 1$$

does the job just as well, but with different boundary conditions at the interfaces, dependent on the values of a and b [13, 17]. The correct choice of the boundary conditions corresponding to a way of ensuring hermiticity of the Hamiltonian other than that given by equations (7) and (8) can be made if one derives the effective-mass Hamiltonian directly from Burt's [18] exact envelope-function theory for semiconductor microstructures, as was done by Foreman [19, 20] and Meney *et al* [21].

Although the 'conventional' boundary conditions do not include correctly the effect of remote bands [21] and overestimate the interband coupling [19], we decided to use equations (7) and (8). The reason for this is that all of the numerical calculations of the subband structure for different growth directions carried out so far by other authors [5–7, 10] were based on this symmetrization of the Hamiltonian. Since the main advantage of our method is the ease with which it allows one to determine the subband structure for any growth direction, it made sense, for the sake of the comparison of results, to obtain them with the same symmetrization of the Hamiltonian as was used by other authors ('conventional' boundary conditions).

Diagonalization of the matrix (6) for a range of values k_1 and k_2 yielded the energy bands $E(k_1, k_2)$ as well as the envelope functions (coefficients $f_{\alpha,n}$). This was done by using the subroutine DEVCHF from IMSL MATH/LIBRARY™ [22].

3. Results

Using the method described in the previous section, we have calculated band structures for several different growth directions. For the direction (001) we were able to calculate a band structure using Chuang's method of block diagonalization [2], and compare the result with that obtained by the present method and those used in [10] and [11].

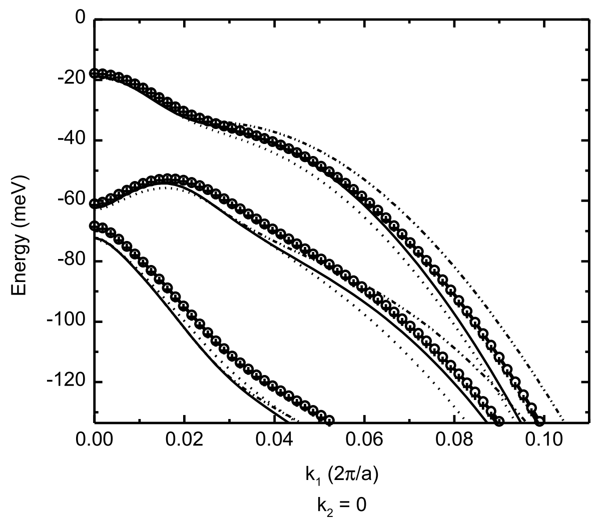

Figure 1. Comparison of subband structures derived by different methods for a $Ga_{0.47}In_{0.53}As$–$In_{0.73}Ga_{0.27}As_{0.58}P_{0.42}$ single quantum well with $L_w = 60$ Å grown in the direction (001); $\gamma_{1w} = 14.031$, $\gamma_{2w} = 5.386$, $\gamma_{3w} = 6.186$, $\gamma_{1b} = 11.698$, $\gamma_{2b} = 4.409$, $\gamma_{3b} = 5.174$; a $= 5.6533$ Å; $N = 55$ plane waves in equations (4*a*)–(4*c*). $- \cdot \cdot -$: $\gamma_j = \gamma_j(\zeta)$, Chuang's method; —○—: $\gamma_j =$ constant (weighted average), $L = 11L_w$; —+—: $\gamma_j =$ constant (weighted average), $L = 6L_w$; ——: $\gamma_j = \gamma_j(\zeta)$, $L = 11L_w$.

From the results shown in figure 1 one can see that the curves derived by the present method and those derived by Chuang's method converge to the same values for $k = 0$. The differences between them show up for larger values of the wave vector. The plane-wave expansion method with constant Luttinger parameters [10], as one could expect, gives results which are dependent on the way in which those constant parameters are determined. A simple arithmetic average for γ_j leads to a better agreement with Chuang's method than the weighted average ($\gamma_j = (\gamma_{jw}L_w + \gamma_{jb}L_b)/L$), the latter giving a significant discrepancy which has already started at $k = 0$.

The results in figure 2 show the band structures for (001), (110), and (111) substrate orientations calculated with the present method. We can see that there are quite different energy band structures for different orientations. Similar curves may be calculated for any arbitrary growth direction using our method, just by specifying θ and φ.

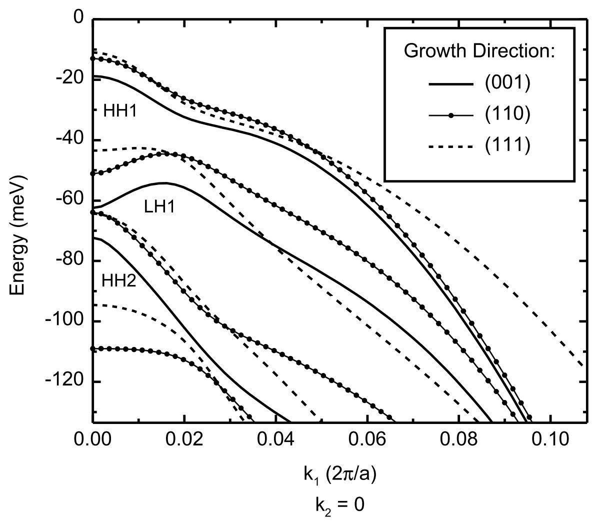

Figure 2. Subband structures obtained by the plane-wave expansion method with $\gamma_j = \gamma_j(\zeta)$ for three different growth directions; the material composition and quantum well width are the same as for figure 1.

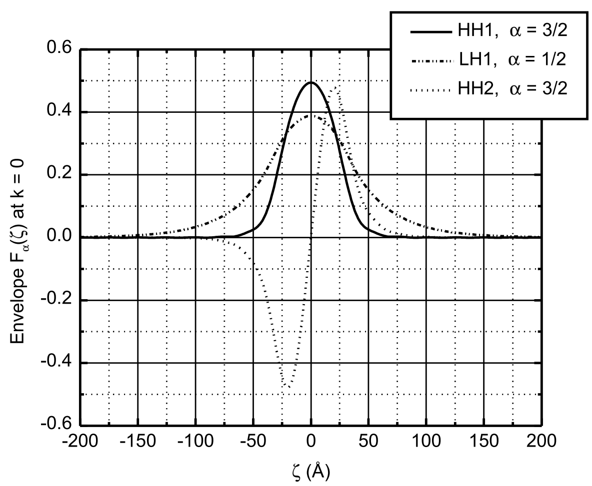

Figure 3. Envelope functions at $k = 0$ for the single-quantum-well system of figure 1.

The method allows one to obtain very easily envelope functions for any direction of growth. The absolute values of the envelope-function components $\mathcal{F}_\alpha(\zeta)$ determine how large the input will be from a given total-angular-momentum eigenfunction to the hole wave function in a subband under consideration. If only one component of the envelope function, for example that with $\alpha = 3/2$, is not identically zero, then the hole wave function (and the corresponding subband) has a well defined heavy-hole character.

For the (001) growth direction and $k = 0$, the only envelope-function components which survive are those shown in figure 3. Consequently one can see that the envelope functions evaluated by the present method show the correct symmetry and give an accurate classification of the energy subbands. Our calculations of the envelope functions for $k \neq 0$ have shown band mixing, i.e. inputs from different total-angular-momentum eigenfunctions to a given hole state.

To get an idea of how the accuracy of the energy eigenvalues depends on the number N of plane waves used in the expansions (4*a*)–(4*c*), we carried out the same numerical calculations with three different numbers of plane waves, namely $N = 55$, $N = 111$, and $N = 223$. The shift of the eigenvalues resulting from the change of N is shown in figure 4. The subband dispersion curves calculated with the three values of N coincide so perfectly that they are indistinguishable on the scales of figures 1 and 2. From examination of figure 5, one can see that the maximum percentage shift of the eigenvalues is well below 0.4%. The tail of the HH2 curve in figure 5 above 0.3% is outside the range of energy of our pictures.

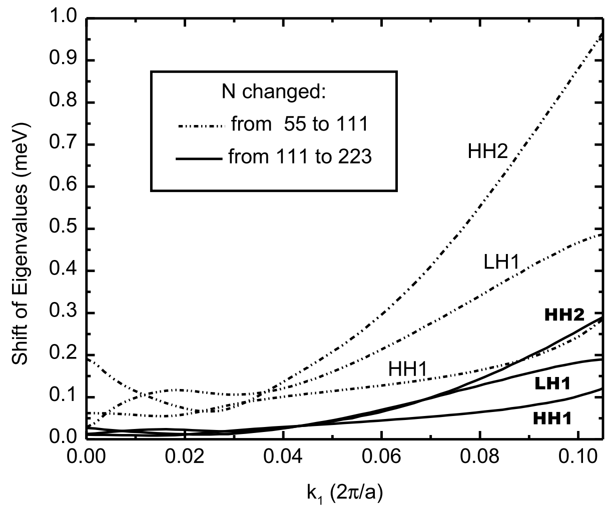

Figure 4. The shift of the eigenvalues of the Hamiltonian (6) as the number of plane waves N in equations (4*a*)–(4*c*) changes from 55 to 223.

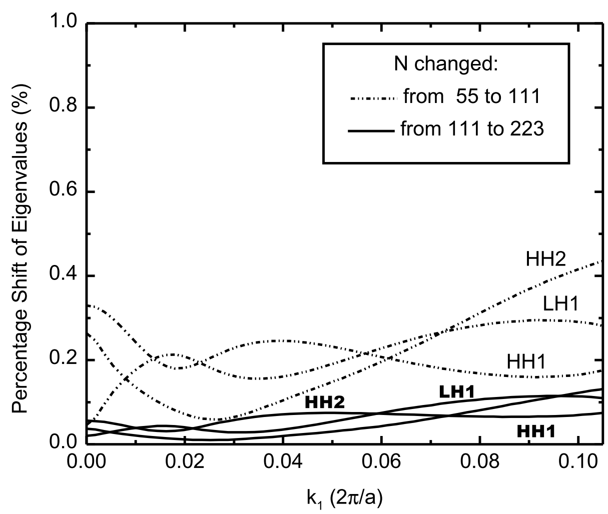

Figure 5. The percentage shift of the eigenvalues of the Hamiltonian (6) as the number of plane waves N in equations (4*a*)–(4*c*) changes from 55 to 223.

It is obvious that using a number of plane waves N slightly larger than 100 should give a sufficient accuracy of hole energies and envelope functions for a single-quantum-well system. This requires the diagonalization of an approximately 400×400 matrix for each value of k, and the calculation time is not a serious problem.

In conclusion, we have developed an efficient numerical method for determining the band structures and envelope wave functions of the Luttinger–Kohn Hamiltonian for different orientations of the substrate. Our method is free from the numerical problems encountered by other methods.

Acknowledgments

We would like to acknowledge support from the Ontario Center for Materials Research (OCMR), the Natural Science and Engineering Research Council of Canada (NSERC), Nortel Technology, and Tampere University of Technology.

Appendix

Each of the 12 matrices in equation (1) has the following form:

$$\mathsf{X} = \begin{bmatrix} X_{1,1} & X_{1,2} & X_{1,3} & 0 \\ X_{1,2}^* & -X_{1,1} & 0 & -X_{1,3} \\ X_{1,3}^* & 0 & -X_{1,1} & X_{1,2} \\ 0 & -X_{1,3}^* & X_{1,2}^* & X_{1,1} \end{bmatrix}.$$

For these matrices, we need to specify only three unique elements, $X_{1,1}$, $X_{1,2}$, and $X_{1,3}$. To write these elements in compact form, we use the following notation:

$$\begin{aligned} c_\theta &\equiv \cos(\theta) \\ s_\theta &\equiv \sin(\theta) \\ c_\varphi &\equiv \cos(\varphi) \\ s_\varphi &\equiv \sin(\varphi). \end{aligned}$$

See table 1 in the text for a listing of the elements.

References

[1] Andreani L C, Pasquarello A and Bassani F 1987 Hole subbands in strained GaAs–$Ga_{1-x}Al_xAs$ quantum wells: exact solution of the effective-mass equation *Phys. Rev.* B **36** 5887–94

[2] Chuang S L 1991 Efficient band-structure calculations of strained quantum wells *Phys. Rev.* B **43** 9649–61

[3] Chuang S L 1995 *Physics of Optoelectronic Devices* (New York: Wiley)

[4] Ahn D, Chuang S L and Chang Y-C 1988 Valence-band mixing effects on the gain and the refractive index change of quantum-well lasers *J. Appl. Phys.* **64** 4056–64

[5] Meney A T 1992 Orientation dependence of subband structure and optical properties in GaAs–GaAlAs quantum wells: [001], [111], [110] and [310] growth directions *Superlatt. Microstruct.* **11** 31–40

[6] Meney A T 1992 Effects of growth direction on lasing performance in GaAs–$Ga_{1-x}Al_xAs$ quantum wells *Superlatt. Microstruct.* **11** 387–92

[7] Los J, Fasolino A and Catellani A 1996 Generalization of the $\vec{k} \cdot \vec{p}$ approach for strained layered semiconductor structures grown on high-index planes *Phys. Rev.* B **53** 4630–48

[8] Altarelli M, Ekenberg U and Fasolino A 1985 Calculation of hole subbands in semiconductor quantum wells and superlattices *Phys. Rev.* B **32** 5138–43

[9] Altarelli M 1983 Electronic structure and semiconductor–semimetal transition in InAs–GaSb superlattices *Phys. Rev.* B **28** 842–5

[10] Xia J-B 1991 Effective-mass theory for superlattices grown on $(11N)$-oriented substrates *Phys. Rev.* B **43** 9856–64

[11] Kucharczyk M and Wartak M S 1998 Orientational dependence of hole effective masses in quantum-well laser structures *Superlatt. Microstruct.* **24** 17

[12] Mathine D L, Myjak S K and Maracas G N 1995 A computational Fourier series solution of the BenDaniel–Duke Hamiltonian for arbitrary shaped quantum wells *IEEE J. Quantum Electron.* **31** 1216–22

[13] Morrow R A and Brownstein K R 1984 Model effective-mass Hamiltonians for abrupt heterojunctions and the associated wave-function-matching conditions *Phys. Rev.* B **30** 678–80

[14] Morrow R A 1987 Establishment of an effective-mass Hamiltonian for abrupt heterojunctions *Phys. Rev.* B **35** 8074–9

[15] Paasch G, Nguyen P H and Gobsch G 1991 Energy-dependent connection rules of envelope functions at heterointerfaces *Phys. Status Solidi* b **167** 581–90

[16] Nojima S 1992 Effects of effective-mass Hamiltonian forms on valence band structures of quantum wells *Japan. J. Appl. Phys.* **31** L1401–3

[17] Brezini A and Sebbanani M 1993 Effective mass theory for abrupt heterostructures *Phys. Status Solidi* b **178** 141–9

[18] Burt M G 1992 The justification for applying the effective-mass approximation to microstructures *J. Phys.: Condens. Matter* **4** 6651–90

[19] Foreman B A 1993 Effective-mass Hamiltonian and boundary conditions for the valence bands of semiconductor microstructures *Phys. Rev.* B **48** 4964–7

[20] Foreman B A 1994 Analytic model for the valence-band structure of strained quantum well **49** 1757–73

[21] Meney A T, Gonul B and Reilly E P 1994 Evaluation of various approximations used in the envelope-function method *Phys. Rev.* B **50** 10 893–904

[22] *User's Manual*: *FORTRAN Subroutines for Mathematical Applications* 1991 IMSL MATH/LIBRARY™, version 2.0